

OPEN

Longitudinal variations in thermospheric parameters under summer noontime conditions inferred from ionospheric observations: A comparison with empirical models

Andrey V. Mikhailov^{1,2} & Loredana Perrone²

Longitudinal variations in the thermospheric neutral composition ($[O]$ and $[N_2]$) and exospheric temperature T_{ex} have been inferred from June monthly median noontime f_oF_1 and f_oF_2 observations at mid-latitudes to check for consistency with empirical MSIS models. In general, a similarity in longitudinal variations has been demonstrated, and this is interesting, as similar variations were obtained with very different methods and different data sources. Both inferred and MSISE-00 modelled height-integrated O/N_2 ratios are comparable to TIMED/GUVI observations only under solar minimum conditions but differ substantially under high solar activity. The retrieved height-integrated O/N_2 ratio longitudinal variations are small ($\sim 15\%$) in comparison to the observed N_mF_2 variations under high solar activity. The height-integrated O/N_2 ratio cannot be incorporated into the F_2 -layer formation mechanism; therefore, such observations cannot be used for any quantitative interpretation of N_mF_2 variations.

Ionospheric parameters during the daytime reflect the state of the surrounding thermosphere and the intensity of incident solar extreme ultraviolet (EUV) radiation; therefore, thermospheric and ionospheric parameters should demonstrate consistent spatial variations. However, historically, global ionospheric IRI¹ and thermospheric models, for instance, MSISE-00² empirical model, have been developed independently of each other, and there is no certainty in their consistency. A direct use of the MSIS model to calculate electron concentration in the ionospheric F region may give unsatisfactory results, and model parameters must be corrected to fit the observed N_mF_2 (electron concentration in the F_2 -layer maximum) under specific geophysical conditions³⁻⁷. Existing global first-principle (physical) models cannot yet compete with empirical models for many reasons^{8,9} and cannot answer the question of consistency between thermospheric models and ionospheric observations.

A recently developed method¹⁰ solving an inverse problem of aeronomy allows us to retrieve a consistent set of main aeronomic parameters responsible for the formation of the daytime mid-latitude ionospheric F-region. Using observed near noontime f_oF_1 and f_oF_2 (critical frequencies of the F_1 and F_2 layers, respectively, related to an electron concentration of $N_e = 1.24 \times 10^4 \text{ fo}^2$) and the standard indices of solar ($F_{10.7}$) and geomagnetic (A_p) activity as the input information, the method¹⁰ provides a neutral composition ($[O]$, $[O_2]$, and $[N_2]$); exospheric temperature T_{ex} ; vertical plasma drift W , which may be converted into effective thermospheric meridional wind V_{nx} ; and total solar EUV flux, with $\lambda \leq 1050 \text{ \AA}$. The inferred aeronomic parameters determine plasma production, as well as its dynamics and recombination at F-region heights. Thus, by solving the inverse problem of aeronomy, we have an opportunity (via the inferred thermospheric parameters) to check the consistency between the observed longitudinal variations in ionospheric parameters (f_oF_1 and f_oF_2) and modern empirical thermospheric

¹Pushkov Institute of Terrestrial Magnetism, Ionosphere and Radio Wave Propagation (IZMIRAN), Moscow, Russia.

²Istituto Nazionale di Geofisica e Vulcanologia (INGV), Rome, Italy. Correspondence and requests for materials should be addressed to L.P. (email: loredana.perrone@ingv.it)

| Station | Lat, N deg | Lon, E deg | Mag. Lat deg | Station | Lat, N deg | Lon, E deg | Mag. Lat deg |
|--------------|------------|------------|--------------|------------|------------|------------|--------------|
| Adak | 51.9 | 183.4 | 47.5 | Ottawa | 45.4 | 284.1 | 56.3 |
| Alma-Ata | 43.2 | 76.9 | 33.3 | Petersburg | 60.0 | 30.7 | 56.0 |
| Boulder | 40.0 | 254.7 | 48.7 | Point Arg | 35.6 | 239.4 | 42.1 |
| Ekaterinburg | 56.7 | 58.6 | 48.6 | Rome | 41.9 | 12.5 | 42.0 |
| Goosebay | 53.3 | 299.6 | 64.1 | Rostov | 47.2 | 39.7 | 42.2 |
| Gorky | 56.1 | 44.2 | 50.0 | Juliusruh | 54.6 | 13.4 | 54.3 |
| Irkutsk | 52.5 | 104.0 | 41.2 | Slough | 51.5 | 359.4 | 53.8 |
| Kaliningrad | 54.7 | 20.6 | 52.7 | St. Johns | 47.6 | 307.3 | 57.9 |
| Karaganda | 49.8 | 73.0 | 40.2 | Tomsk | 56.5 | 84.9 | 45.9 |
| Kiev | 50.5 | 30.5 | 46.9 | Tunguska | 61.6 | 90.0 | 50.7 |
| Kokubunji | 35.7 | 139.5 | 25.7 | Wakkanai | 45.4 | 141.7 | 35.5 |
| Magadan | 60.1 | 151.0 | 50.9 | Winnipeg | 49.8 | 265.6 | 59.6 |
| Moscow | 55.5 | 37.3 | 50.6 | Yakutsk | 62.0 | 129.6 | 51.2 |

Table 1. Stations with available June monthly median f_oF_1 and f_oF_2 observations used in the analysis. Geographic latitudes, longitudes and magnetic latitudes of the stations are given.

models. Unlike recent analyses of longitudinal variations dealing with integrated thermospheric characteristics, such as neutral gas density¹¹ or height-integrated O/N₂ ratio¹², the proposed method provides individual thermospheric parameters ([O], [O₂], [N₂], and T_{ex}). The electron concentration in the maximum of the F₂-layer (N_mF₂) depends on individual [O] and [N₂] concentrations rather than on the height-integrated O/N₂ ratio, as is suggested in some publications¹³. In the beginning of the space era, thermospheric neutral composition ([O] and [N₂]) was measured with mass- spectrometers, and these two species were shown to demonstrate different spatial variations¹⁴.

The aims of the paper may be formulated as follows:

- To analyse longitudinal variations in available noontime monthly median f_oF_1 and f_oF_2 observations for June under solar minimum and maximum conditions;
- To retrieve thermospheric parameters from f_oF_1 and f_oF_2 observations and to analyse their longitudinal variations in comparison with the empirical thermospheric models to check the consistency between them;
- To discuss the physical mechanism of the longitudinal variations in thermospheric and ionospheric parameters under June noontime conditions while considering the inferred neutral composition and recent height-integrated O/N₂ ratio observations.

Method

The method used in our analysis was described in a previous paper¹⁰. It is based on solving an inverse problem of aeronomy. The idea is to use routine ground-based f_oF_1 (or f_{0180} - plasma frequency at a 180 km height) and f_oF_2 near-noontime observations to find a consistent set of main aeronomic parameters responsible for the F-region formation under given geophysical conditions. The method has two versions that are used depending on the available input information. As long as we consider historical monthly median ionospheric observations, only summer f_oF_1 data are available, and we use June f_oF_1 observations when the F₁ layer is distinct on ionograms and gaps in the data are practically absent. Historical monthly median electron density profiles Ne(h) used to read f_{0180} are absent. Daytime (10–14 LT) monthly median N_mF₂ and N_mF₁ observed by the worldwide ground-based ionosonde network in the Northern Hemisphere were used in our analysis. Such observations are available for 50–70 years at some stations.

By solving continuity equations for the main ionospheric ions and applying the method of multi-parametric optimization¹⁵, it is possible to fit the calculated N_mF₂ and N_mF₁ to the observed ones and to infer factors for the MSIS-86 model exospheric temperature T_{ex}, neutral composition ([O], [O₂], and [N₂]), and the total solar ionizing EUV flux with $\lambda \leq 1050$ Å from the model¹⁶. Under known neutral composition and temperature, the vertical plasma drift W can be obtained by fitting the calculated N_mF₂ to the observed one. In fact, all aeronomic parameters are found simultaneously in the iterations. The method was tested using CHAMP/STAR neutral gas density observations under various geophysical conditions, and it was shown to demonstrate advantages over modern empirical thermospheric models¹⁰.

Results

An inspection of available simultaneous f_oF_1 and f_oF_2 June noontime observations over the Northern Hemisphere has shown that the largest amount of data was available in 1975, 1976, 1985, and 1986 for the solar minimum and in 1969, 1970, 1980, and 1981 for the solar maximum. Observations at 26 mid-latitude stations (<http://spidr.ngdc.noaa.gov/spidr/>) were used in our analysis (Table 1).

Observations were grouped by years with solar minima and maxima. Before this grouping, the observed f_oF_1 and f_oF_2 were reduced to the same latitude of 50°N and the same level of solar activity using the internal structure of the IRI model. The IRI model dependences of f_oF_1 and f_oF_2 on coordinates and solar activity were used

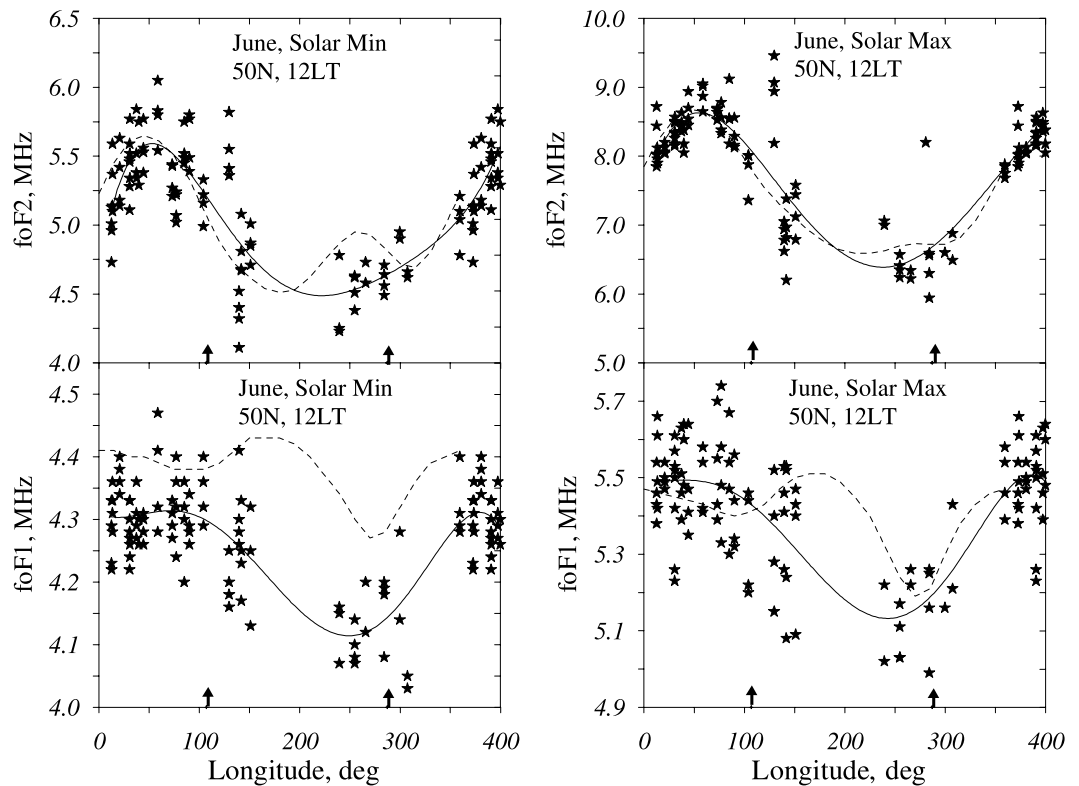


Figure 1. Longitudinal variations in reduced f_oF_2 and f_oF_1 for solar minimums and maximums are given in a comparison with the IRI-2016 model (dashes). Solid curves are polynomial approximations. Points from 0° – 40° E are repeated at 360° – 400° E longitudes. Arrows indicate the longitude of the geomagnetic pole meridian.

for this reduction. The input index of solar activity to the IRI is a 12-month running mean sunspot number R_{12} or a 12-month running mean index $F_{10.7}$ (F_{12}), which is averaged for June over the years with a solar minimum $R_{12} = 15$ ($F_{12} = 75$) and for the years with a solar maximum $R_{12} = 125$ ($F_{12} = 177$).

The reduced f_oF_2 and f_oF_1 are given in Fig. 1 in comparison to the IRI-2016 (https://ccmc.gsfc.nasa.gov/modelweb/models/iri2016_vitmo.php) model variations. Pronounced f_oF_2 and f_oF_1 longitudinal variations are observed under both levels of solar activity. The IRI-2016 model describes the observed f_oF_2 with sufficient accuracy, while the f_oF_1 model values are overestimated under solar minimum.

The interpolated positions of maxima at 50° – 60° E and minima at 240° – 250° E are very close for f_oF_2 and f_oF_1 (Fig. 1), but they do not coincide with the longitude of the magnetic pole or the λ_{pol} and $(\lambda_{\text{pol}} + 180^\circ)$ longitudes. The extrema are shifted to the west with respect to the magnetic pole meridian. Ionospheric F₁ and F₂ layers have different formation mechanisms, but they both depend on the same neutral composition, and the coincidence of extreme positions confirms the controlling role of neutral composition in longitudinal variations.

The application of method¹⁰ to ionospheric observations at 26 stations has given us neutral temperature and composition at F-region heights (>140 km). The retrieved neutral composition and temperature were reduced to the same latitude of 50° N and fixed levels of solar activity using the MSIS-86 model¹⁷ internal structure. The input June monthly $F_{10.7}$ and A_p indices averaged over the years of solar minimum are $F_{10.7} = 71$ and $A_p = 10$ nT and $F_{10.7} = 167$ and $A_p = 11$ nT for years with a solar maximum. When reduced this way, [O], [N₂], O/N₂ ratio, and Tex are given in Fig. 2 for the solar minimum and maximum in a comparison to thermospheric models MSIS-86 and MSISE-00.

Both the retrieved and modelled values manifest pronounced longitudinal variations (Fig. 2). The extrema are located at 50° – 60° E and 240° – 250° E with similar f_oF_1 and f_oF_2 variations (Fig. 1). This coincidence is not surprising, as daytime f_oF_2 and f_oF_1 reflect corresponding variations in the thermospheric parameters. The extrema in Fig. 2 are also shifted to the west with respect to the magnetic pole meridian. In general, MSISE-00 (which has nothing in common with the retrieval method) is closer to the retrieved variations in thermospheric parameters compared to MSIS-86. Although the model and retrieved longitudinal variations appear very similar, the absolute differences are also observed. Modelled Tex values are systematically larger than the inferred ones, especially with MSIS-86. This results in larger [N₂] concentrations, especially in the American longitudinal sector. It is interesting to note that despite noticeable differences in Tex, [N₂], and [O] between the two versions of the MSIS model, the longitudinal variations in the O/N₂ ratio are very similar (Fig. 2).

The similarity between the retrieved and modelled longitudinal variations in thermospheric parameters looks interesting, as the compared variations were obtained with very different methods using very different source data. This similarity is also confirmed by the relative (maximum/minimum ratio) variations given in Table 2. Perfect coincidence is observed for the O/N₂ ratio under both levels of solar activity and for other parameters

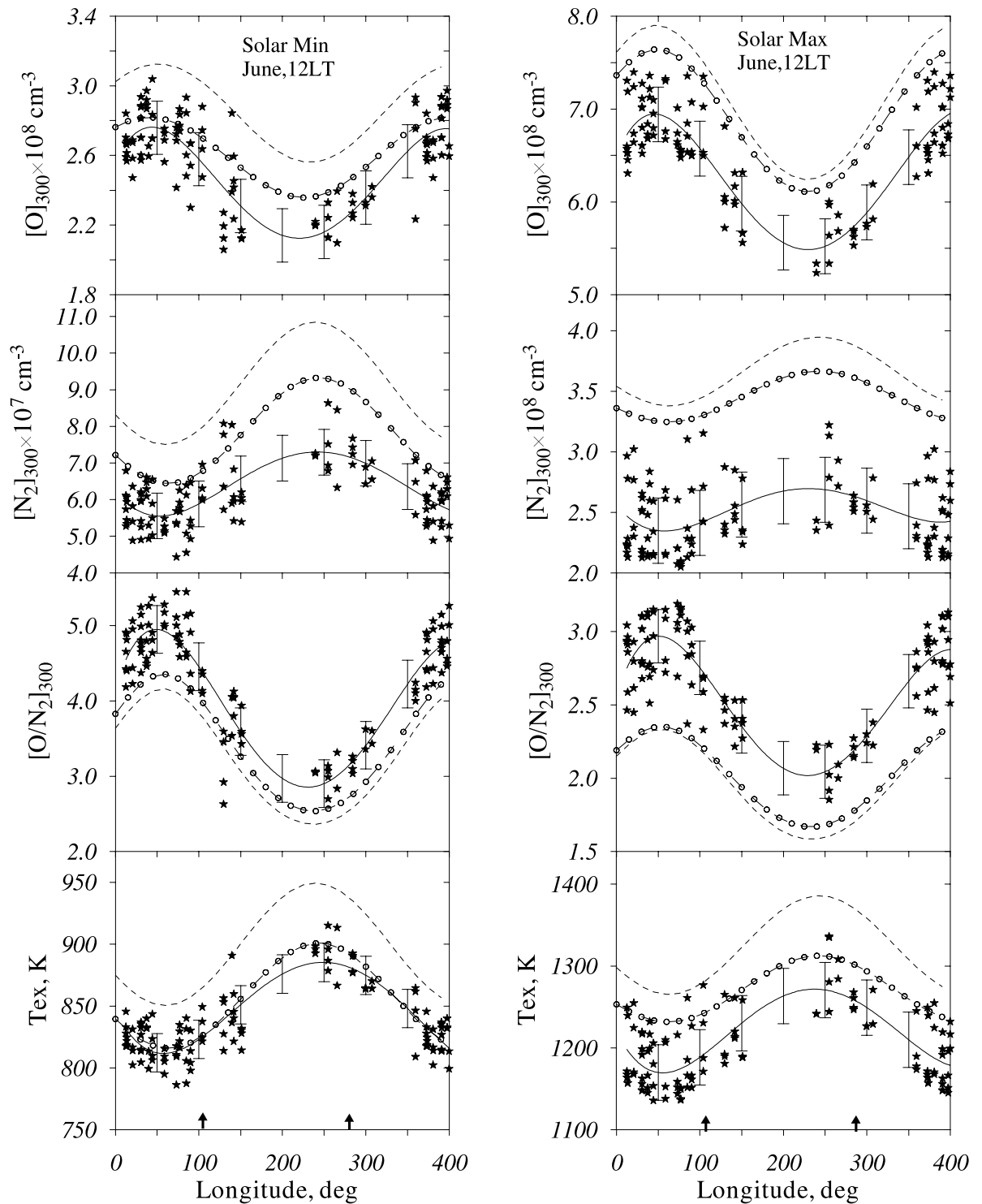


Figure 2. Longitudinal variations in the inferred thermospheric parameters at 300 km and 50°N for years with a solar minimum and maximum. Solid lines – polynomial approximations with error bars (SD values are given); dashes – MSIS-86 model; and circles – MSISE-00 model. Points from 0°–40°E are repeated at 360°–400°E longitudes. Arrows indicate the longitude of the geomagnetic pole meridian.

under solar maximum conditions. The largest difference occurs for atomic oxygen under a solar minimum when MSISE-00 underestimates the magnitude of [O] longitudinal variations (also Fig. 2). This is mainly due to lower [O] values in the American longitudinal sector.

| Parameter | Solar minimum | | | Solar maximum | | |
|-------------------|---------------|---------|----------|---------------|---------|----------|
| | Retrieved | MSIS-86 | MSISE-00 | Retrieved | MSIS-86 | MSISE-00 |
| [O] | 1.30 | 1.22 | 1.19 | 1.27 | 1.27 | 1.25 |
| [N ₂] | 1.31 | 1.44 | 1.45 | 1.15 | 1.17 | 1.13 |
| O/N ₂ | 1.73 | 1.76 | 1.71 | 1.47 | 1.47 | 1.41 |
| T _{ex} | 1.09 | 1.12 | 1.10 | 1.09 | 1.09 | 1.06 |

Table 2. Magnitudes of longitudinal variations for the retrieved and modelled thermospheric parameters at 300 km, 50°N, and 12 LT in June during solar minimum and maximum conditions.

| Years | Stations | N _m F ₂ × 10 ⁵ , cm ⁻³ | N _m F ₂ × 10 ⁵ , cm ⁻³ (IRI) |
|-------|---------------------|--|---|
| 2009 | Rome | 3.22 | 3.51 |
| | Juliusruh | 2.87 | 2.74 |
| | Boulder | 2.86 | 2.87 |
| | Millst. Hill | 2.62 | 2.87 |
| 2000 | Rome | 10.71 | 9.56 |
| | Juliusruh | 6.76 | 6.43 |
| | Boulder | 5.78 | 6.54 |
| | Millst. Hill | 6.60 | 6.07 |

Table 3. Observations and IRI model results of June noontime monthly median N_mF₂ for solar minimum (2009) and maximum (2000) years.

Discussion

From the very beginning, the mechanism of longitudinal/UT variations in neutral composition has been associated with high-latitude heating and displacement between the geomagnetic and geographic poles^{14,18,19}. Due to Joule and particle precipitation heating in the auroral zone, the upper atmosphere expands, and this upwelling results in a decrease in the O/N₂ ratio at a fixed height. Equatorward solar driven and/or disturbed thermospheric circulation transfers this disturbed neutral composition to lower latitudes. This mechanism has been discussed in the literature^{20–22}. The near-to-pole longitudinal (American) sector should manifest larger [N₂] and lower [O] and O/N₂ compared to the European sector at the same geographic latitudes, as shown in Fig. 2. The reduction in the retrieved thermospheric parameters at the same geomagnetic latitude $\Phi = 50^\circ$ (not shown in the paper) only slightly changes the pattern of longitudinal variations, shifting the extrema farther to the west.

One may conclude that June auroral heating is systematically larger in the American sector. A plausible explanation for this extra heating is the larger Joule heating due to the larger conductivity in the auroral zone. The auroral oval (<http://www.sws.bom.gov.au/Aurora/3/1>) receives more sunlight in June in the American sector than in the European sector. The noontime solar zenith angle χ is 42° at the longitude of the magnetic pole (73°W), but noontime χ is 61° at the antipode longitude of 107°E. Considering the electron concentration in the E-region²³ $N_m E \sim (\cos \chi)^{0.6}$, the expected difference in the electron concentration is ~30%, which provides a larger conductivity.

A westward shift in the extrema of the longitudinal variations with respect to the longitude of the magnetic pole meridian taking place both in the ionospheric (Fig. 1) and retrieved parameters, as well as in the modelled thermospheric parameters (Fig. 2), reveals the reality of this shift, which may be related to dominating westward circulation at mid-latitudes during the June solstice²⁴. A westward tilt was also observed in the mean thermospheric mass density¹¹.

Longitudinal variations in the daytime column O/N₂ ratio from TIMED/GUVI observations on solstices were analysed by the authors¹². The column O/N₂ ratio in those observations²⁵ was calculated above the level where the column N₂ abundance of 10¹⁷ cm⁻² was located at a 147–150 km height. It is interesting to compare the observed column O/N₂ ratio to our retrieved and MSISE-00 modelled longitudinal/solar activity variations. For this comparison, we selected stations with close geographic latitudes, Rome (41.9°N, 12.5°E; $\Phi = 42^\circ$) and Boulder (40.0°N, 254.7°E; $\Phi = 48.5^\circ$), and a pair of stations with close geomagnetic latitudes, Juliusruh (54.6°N, 13.4°E; $\Phi = 54^\circ$) and Millstone Hill (42.5°N, 288.5°E; $\Phi = 53.3^\circ$), which are located in the European and American longitudinal sectors, respectively. The last deep solar minimum in 2009 ($F_{10.7} = 68.6$; $A_p = 4.1$) and solar maximum in 2000 ($F_{10.7} = 179.8$; $A_p = 15.2$) were taken for our analysis, where $F_{10.7}$ and A_p are June monthly indices. Observed June noontime monthly median N_mF₂ values are given in a comparison to IRI-2016 values to show that the selected stations manifest N_mF₂ similar to the modelled results. (Table 3)

The observed monthly median $f_o F_2$ and $f_o F_1$ at the four stations were used to retrieve thermospheric parameters and calculate column O/N₂ ratios above the level with a column N₂ abundance of 10¹⁷ cm⁻², as was done in the observations¹². Table 4 gives a comparison with the MSISE-00 modelled column O/N₂ ratios.

Table 4 shows that both the inferred and MSISE-00 modelled height-integrated O/N₂ ratios increase with solar activity. Our results and the MSISE-00 values are comparable with the TIMED/GUVI observations¹² at 12 LT in June under solar minimum conditions at ~45°N with a column O/N₂ ratio ~ 0.5. However, the TIMED/GUVI

| Station | 2009 | 2000 |
|--------------|---------------|---------------|
| Rome | 0.632 (0.551) | 0.802 (0.701) |
| Juliusruh | 0.514 (0.476) | 0.682 (0.588) |
| Boulder | 0.554 (0.460) | 0.696 (0.606) |
| Millst. Hill | 0.507 (0.465) | 0.694 (0.598) |

Table 4. Inferred and MSISE-00 model (in parentheses) height-integrated June noontime O/N₂ ratios in the European and American sectors under solar maximum (2000) and minimum (2009) monthly median conditions.

| Parameter | Rome | Boulder | Juliusruh | Millstone Hill |
|--|--------------|--------------|----------------|----------------|
| [O] _{col} × 10 ¹⁷ , cm ⁻² | 8.12 7.69 | 7.13 6.54 | 6.39 6.14 | 6.90 6.45 |
| [N ₂] _{col} × 10 ²⁰ , cm ⁻² | 9.81 9.79 | 9.65 9.63 | 10.96 10.93 | 9.84 9.82 |
| Tex, K | 1265 781 | 1308 817 | 1296 805 | 1312 816 |
| T ₇₀ , K | 209 209 | 210 210 | 210 210 | 209 209 |

Table 5. MSISE-00 modelled total column contents of [O] and [N₂] above 70 km under solar maximum (2000, first line) and solar minimum (2009, second line) conditions, in addition to Tex and neutral temperature at a 70 km height, at four locations.

observations manifest the inverse dependence on solar activity, and the observed height-integrated O/N₂ ratio is <0.4 at ~45°N under high solar activity¹² (their Fig. 4), while our inferred and MSISE-00 column O/N₂ ratios are 0.6–0.8 in 2000 (Table 4). On the other hand, qualitatively TIMED/GUVI observations demonstrate correct longitudinal variations with a larger column O/N₂ ratio in the European sector compared to the American sector in accordance with our results and the MSISE-00 model results.

The increase in the retrieved and MSISE-00 modelled height-integrated O/N₂ ratio with solar activity indicates an increase in atomic oxygen abundance under solar maximum conditions. This is determined from the following. Above the turbopause, which is located at 110–120 km (while the level with column N₂ content of 10¹⁷ cm⁻² is at ~150 km), the neutral species are distributed in accordance with the barometric law; therefore, the column content of any species above the height *h* is N_hH, where N_h is the concentration and H is the scale height *kT/mg* of a given species. Therefore, the O/N₂ column ratio is independent of neutral gas temperature but depends only on the [O]/[N₂] ratio at a fixed height *h*. Atomic oxygen is completely produced and lost in the upper atmosphere²⁶, forming a layer with a maximum at ~97 km and zero concentrations below 80 km²⁷. Therefore, height-integrated [O] above 70 km gives the total column content of atomic oxygen. Table 5 gives the MSISE-00 modelled total column contents of [O] and [N₂] above 70 km under solar maximum (2000) and solar minimum (2009) conditions, in addition to Tex and neutral temperature at a 70 km height, at four locations.

Table 5 shows a 4–9% increase in the [O] column content in 2000 compared to 2009, while [N₂]_{col} is practically unchanged. The increase in the atomic oxygen abundance under high solar activity may be attributed to an increase in the intensity of the Schumann-Runge continuum, which is responsible for the dissociation of O₂ in the upper atmosphere. The stability of the MSISE-00 modelled [N₂]_{col} under varying solar activity is due to relatively stable neutral temperatures at mesospheric heights, which provide the main contribution to the [N₂] column content (Table 5).

The TIMED/GUVI height-integrated O/N₂ ratios are sometimes used to interpret global-scale seasonal and solar activity N_mF₂ variations¹³. Indeed, a simplified formation mechanism of the mid-latitude daytime F₂-layer, ignoring vertical plasma drift, may be related to the O/N₂ ratio taken at the F₂-layer maximum height²⁸

$$N_m F_2 = 0.75 \frac{q_m}{\beta_m}$$

where *q_m* is the O⁺ ion production rate and β_m is the linear loss coefficient taken at *h_mF₂*. With some reservations, *q_m/β_m* may be considered to be proportional to (O/N₂)_{max}, but this ratio taken at *h_mF₂* is not the same as the height-integrated O/N₂ ratio. Our method¹⁰ provides the necessary *h_mF₂* to calculate (O/N₂)_{max}. Table 6 gives the Rome/Millstone Hill and Rome/Boulder ratios for the observed N_mF₂, (O/N₂)_{max} and (O/N₂)_{col} ratios for the two levels of solar activity.

Table 6 shows that (O/N₂)_{col} longitudinal variations are small (~15%) in comparison with the observed N_mF₂ variations under high solar activity. They are close only during the deep solar minimum in 2009, while the (O/N₂)_{max} longitudinal variations are much closer to the observed N_mF₂ variations under both solar activity conditions. This is not a surprise, as the level with a N₂ column density of 10¹⁷ cm⁻² (used to calculate the column O/N₂ ratio) is located at heights of 147–150 km, i.e., much further below the F₂-layer maximum; however, these concentrations provide the main contribution to the column density, but they do not participate in the F₂-layer formation.

| Parameter | 2009 | | 2000 | |
|--------------------------------|---------------------|------------------|---------------------|------------------|
| | Rome/ Mill. Hill | Rome/ Boulder | Rome/ Mill. Hill | Rome/ Boulder |
| $\Delta(N_m F_2)_{\text{obs}}$ | 1.23 | 1.13 | 1.62 | 1.85 |
| $\Delta(O/N_2)_{\text{max}}$ | 1.27 | 1.00 | 1.49 | 1.97 |
| $\Delta(O/N_2)_{\text{col}}$ | 1.25 | 1.14 | 1.16 | 1.15 |

Table 6. Rome/Millstone Hill and Rome/Boulder ratios for observed $N_m F_2$, retrieved O/N_2 ratio at $h_m F_2$, and column O/N_2 ratio calculated from the retrieved $[O]$ and $[N_2]$ for June 2009 and 2000.

Another problem with using the column (O/N_2) ratio to interpret any spatial, seasonal, or solar activity $N_m F_2$ variations is the smoothing temperature effect. The atomic oxygen concentration is a crucial parameter for F_2 -region formation as $N_m F_2 \sim [O]^{4/3}$ during daytime hours²⁹. Its concentration in the American sector is 30% less than that in the Eurasian sector (Table 2), and this difference is mainly responsible for the observed $N_m F_2$ longitudinal variations. However, T_{ex} and, correspondingly, the atomic oxygen scale height are larger in the American sector (Fig. 2), which decreases the difference in the height-integrated O/N_2 ratios between the two sectors. Keeping all of this in mind, one may conclude that the column O/N_2 ratio cannot be used for any quantitative interpretation of $N_m F_2$ variations.

Conclusions

The obtained results are summarized as follows.

1. The observed longitudinal $f_o F_1$ and $f_o F_2$ variations are similar to the retrieved and MSIS modelled thermospheric parameter variations, indicating their general consistency. The best coincidence with the empirical models is related to the inferred O/N_2 ratio, while MSISE-00 underestimates the magnitude of $[O]$ longitudinal variations under solar minimum conditions. In general, similar variations in thermospheric parameters obtained with different methods and different data sources are interesting.
2. The American sector manifests larger T_{ex} values (independent of both the geographic and geomagnetic latitudes considered) under both solar maximum and minimum conditions. A plausible explanation for this extra heating is the larger conductivity in the auroral oval, which receives more sunlight in June in the American sector compared to the European sector.
3. A westward shift in the extreme position in terms of longitudinal variations with respect to the longitude of the magnetic pole meridian, taking place both for ionospheric and thermospheric parameters, may be related to dominating westward circulation at mid-latitudes during the June solstice²⁴.
4. The inferred and MSISE-00 height-integrated O/N_2 ratios are comparable to the TIMED/GUVI observations only under solar minimum conditions, with a column O/N_2 ratio ~ 0.5 at 12 LT in June at $\sim 45^\circ N$ ¹² (their Fig. 2). However, the TIMED/GUVI observations manifest an inverse dependence on solar activity with a height-integrated O/N_2 ratio < 0.4 under high solar activity, which is contrary to the retrieved and MSISE-00 modelled column O/N_2 ratios (0.6–0.8).
5. The retrieved height-integrated (O/N_2) ratio longitudinal variations are small ($\sim 15\%$) in comparison with the observed $N_m F_2$ variations under high solar activity. A 30% difference in atomic oxygen concentration between the American and European sectors is mainly responsible for the observed $N_m F_2$ longitudinal variations and is strongly compensated in $(O/N_2)_{\text{col}}$ by a larger T_{ex} in the American sector. The height-integrated O/N_2 ratio cannot be incorporated into the F_2 -layer formation mechanism; therefore, such observations cannot be used for any quantitative interpretation of $N_m F_2$ variations.

References

1. Bilitza, D. *et al.* International Reference Ionosphere 2016: From ionospheric climate to real-time weather predictions. *Space Weather* **15**, 418–429 (2017).
2. Picone, J. M., Hedin, A. E., Drob, D. P. & Aikin, A. C. NRLMSISE-00 empirical model of the atmosphere: Statistical comparison and scientific issues. *Journal of Geophysical Research: Space Physics* **107**, 1468 (2002).
3. Richards, P. G., Torr, D. G., Buonsanto, M. J. & Miller, K. L. The behavior of the electron density and temperature at Millstone Hill during the equinox transition study September 1984. *J. Geophys. Res.* **94**, 16,969–16,975 (1989).
4. Richards, P. G., Torr, D. G., Buonsanto, M. J. & Sipler, D. Ionospheric effects of the March 1990 magnetic storm: comparison of theory and measurement. *J. Geophys. Res.* **99**, 23,359–23,365 (1994).
5. Richards, P. G. & Wilkinson, P. J. The ionosphere and thermosphere at southern midlatitudes during the November 1993 ionospheric storm: A comparison of measurement and modeling. *J. Geophys. Res.* **103**, 9373–9389 (1998).
6. Pavlov, A. V. & Foster, J. C. Model/data comparison of F region ionospheric perturbation over Millstone Hill during the severe geomagnetic storm of July 15–16, 2000. *J. Geophys. Res.* **106**(A12), 29,051–29,069 (2001).
7. Richards, P. G. Seasonal and solar cycle variations of the ionospheric peak electron density: Comparison of measurement and models. *J. Geophys. Res.* **106**(A7), 12,803–12,819 (2001).
8. Shim, J. S. *et al.* CEDAR Electrodynamics Thermosphere Ionosphere (ETI) Challenge for systematic assessment of ionosphere/thermosphere models: NmF2, and hmF2, and vertical drift using ground-based observations. *Space Weather* **9**, S12003 (2011).
9. Shim, J. S. *et al.* CEDAR Electrodynamics Thermosphere Ionosphere (ETI) Challenge for systematic assessment of ionosphere/thermosphere models: Electron density, neutral density, NmF2, and hmF2 using space based observations. *Space Weather* **10**, S10004 (2012).
10. Perrone, L. & Mikhailov, A. V. A New Method to Retrieve Thermospheric Parameters From Daytime Bottom-Side Ne(h) Observations. *Journal of Geophysical Research: Space Physics* **123**, 10,200–10,212 (2018).
11. Xu, J., Wang, W. & Gao, H. The longitudinal variation of the daily mean thermospheric mass density. *J. Geophys. Res. Space Physics* **118**, 515–523 (2013).

12. Luan, X., Wang, W., Burns, A. & Dou, X. Solar cycle variations of thermospheric O/N₂ longitudinal pattern from TIMED/GUVI. *J. Geophys. Res. Space Physics* **122**, 2605–2618 (2017).
13. Burns, A. G. *et al.* On the solar cycle variation of the winter anomaly. *J. Geophys. Res. Space Physics* **119**, 4938–4949 (2014).
14. Laux, U. & von Zahn, U. Longitudinal Variations in Thermospheric Composition Under Geomagnetically Quiet Conditions. *J. Geophys. Res.* **84**, 1942–1946 (1979).
15. Himmelblau, D. M. *Applied Nonlinear Programming*, (McGraw-Hill Book Company, 1972).
16. Nusinov, A. A. Models for prediction of EUV and X-ray solar radiation based on 10.7-cm radio emission., Proc. Workshop on Solar Electromagnetic Radiation for Solar Cycle 22, Boulder, Co., July 1992, Ed. R.F. Donnelly, NOAA ERL, Boulder, Co., USA, 354–359 (1992).
17. Hedin, A. E. MSIS-86 thermospheric model. *J. Geophys. Res.* **92**, 4649–4662 (1987).
18. Hedin, A. E. & Reber, C. A. Longitudinal variations of thermospheric composition indicating magnetic control of polar heat input. *J. Geophys. Res.* **77**, 2871–2878 (1972).
19. Reber, C. A. & Hedin, A. E. Heating of the high-latitude thermosphere during magnetically quiet periods. *J. Geophys. Res.* **79**, 2457–2461 (1974).
20. Pröhl, G. W. *Ionospheric F-region storms, Handbook of Atmospheric Electrodynamics*, Vol. 2 (ed. Volland), CRC Press/Boca Raton, pp. 195–248 (1995).
21. Rishbeth, H. How the thermospheric circulation affects the ionospheric F₂-layer. *J. Atmos. Sol. Terr. Phys.* **60**, 1385–1402 (1998).
22. Rishbeth, H. & Müller-Wodarg, I. C. F. Vertical circulation and thermospheric composition: a modelling study. *Ann. Geophysicae.* **17**, 794–805 (1999).
23. Kouris, S. S. & Muggleton, L. M. Diurnal variation in the E-layer ionization. *J. Atmos. Terr. Phys.* **35**, 133–139 (1973).
24. Drob, D. P. *et al.* An update to the Horizontal Wind Model (HWM): The quiet time Thermosphere. *Earth and Space Science* **2**, 301–319 (2015).
25. Zhang, Y. *et al.* O/N₂ changes during 1–4 October 2002 storms: IMAGE SI-13 and TIMED/GUVI observations. *J. Geophys. Res.* **109**, A10308 (2004).
26. Banks, P. M., & Kockarts, G. *Aeronomy*, (Academic Press, New York, London, 1973).
27. Mlynarczyk, M. G. *et al.* Atomic oxygen in the mesosphere and lower thermosphere derived from SABER: Algorithm theoretical basis and measurement uncertainty. *J. Geophys. Res. Atmos.* **118**, <https://doi.org/10.1002/jgrd.50401> (2013).
28. Rishbeth, H. & Barron, D. W. Equilibrium electron distributions in the ionospheric F₂-layer. *J. Atmos. Terr. Phys.* **18**, 234–252 (1960).
29. Mikhailov, A. V., Skoblin, M. G. & Förster, M. Day-time F₂-layer positive storm effect at middle and lower latitudes. *Ann. Geophys.* **13**, 532–540 (1995).

Author Contributions

The paper is the result of common investigations. A. Mikhailov conceived the study and contribute to the data analysis and to the preparation and finalization of the manuscript. L. Perrone contribute to the data analysis and to the preparation and finalization of the manuscript.

Additional Information

Competing Interests: The authors declare no competing interests.

Publisher's note: Springer Nature remains neutral with regard to jurisdictional claims in published maps and institutional affiliations.



Open Access This article is licensed under a Creative Commons Attribution 4.0 International License, which permits use, sharing, adaptation, distribution and reproduction in any medium or format, as long as you give appropriate credit to the original author(s) and the source, provide a link to the Creative Commons license, and indicate if changes were made. The images or other third party material in this article are included in the article's Creative Commons license, unless indicated otherwise in a credit line to the material. If material is not included in the article's Creative Commons license and your intended use is not permitted by statutory regulation or exceeds the permitted use, you will need to obtain permission directly from the copyright holder. To view a copy of this license, visit <http://creativecommons.org/licenses/by/4.0/>.

© The Author(s) 2019